

Article

# Photocatalytic and Photostability Behavior of Ag- and/or Al-Doped ZnO Films in Methylene Blue and Rhodamine B under UV-C Irradiation

Adeel Riaz <sup>1</sup>, Amna Ashraf <sup>1</sup>, Hymna Taimoor <sup>1</sup>, Sofia Javed <sup>1</sup> , Muhammad Aftab Akram <sup>1</sup> ,  
Mohammad Islam <sup>2,\*</sup> , Mohammad Mujahid <sup>1</sup>, Iftikhar Ahmad <sup>2</sup> and Khalid Saeed <sup>3</sup>

- <sup>1</sup> School of Chemical and Materials Engineering, National University of Sciences and Technology, Islamabad 44000, Pakistan; adeelriaz03@gmail.com (A.R.); amnaashraf04@hotmail.com (A.A.); hymnataimoor94@live.com (H.T.); sofia.javed@scme.nust.edu.pk (S.J.); aftabakram@scme.nust.edu.pk (M.A.A.); drmmujahid@gmail.com (M.M.)
- <sup>2</sup> Center of Excellence for Research in Engineering Materials (CEREM), Deanship of Scientific Research, King Saud University, P.O. Box 800, Riyadh 11421, Saudi Arabia; ifahmad@ksu.edu.sa
- <sup>3</sup> Department of Mechanical Engineering, College of Engineering, King Saud University, P.O. Box 800, Riyadh 11421, Saudi Arabia; khaliduetp@gmail.com
- \* Correspondence: miqureshi@ksu.edu.sa; Tel.: +966-544523909

Received: 25 February 2019; Accepted: 18 March 2019; Published: 20 March 2019



**Abstract:** Silver (Ag) and/or aluminum (Al)-doped zinc oxide (ZnO:Ag, ZnO:Al) films with different concentrations were produced using sol-gel process and investigated for wettability and photocatalysis. Water contact angle (CA) measurements indicated the films to be hydrophilic with reduced solid/liquid interfacial surface energy upon metal doping. The films were highly transparent (>94%) with red or blue shift in the absorption edge depending on the dopant type (Ag or Al) owing to the Burstein–Moss effect. The ZnO:Ag and ZnO:Al films with 0.5 and 1.0 wt.% metal dopant showed high degradation efficiency in methylene blue (MB) solution under UV irradiation, mainly due to an increase in the photogenerated electron–hole pair recombination time and hydroxyl radicals ( $\cdot\text{OH}$ ) generation. The MB degradation followed pseudo-first-order reaction with maximum apparent reaction rate constant of  $2.40\text{ h}^{-1}$  for the 0.5 wt.% ZnO:Al film. ZnO films with 1.0 wt.% dopant demonstrated excellent photostability and recyclability even after several runs presumably due to reduced  $\text{Zn}^{2+}$  dissolution as well as blocking of the active surface area. ZnO:(Ag + Al) film containing 0.5 wt.% Al and Ag showed excellent UV photodegradation of MB and rhodamine blue (RhB) with high levels of photostability over five cycles.

**Keywords:** zinc oxide films; photocatalysis; methylene blue; photostability; contact angle; rhodamine B

## 1. Introduction

Nanostructured semiconductor thin films have gained increasing interest as self-cleaning surfaces over the last decade [1,2]. This is due to their commercialization prospects [3–5] and extensive practical applications such as window glass [3,6], fabrics [6], paints [7], construction materials [8], plastics [9], solar cells [10] and environmental remediation [11]. In principle, the self-cleaning process can employ hydrophilic or hydrophobic surfaces. In the former case, self-cleaning is achieved through either of the two mechanisms, namely the sheeting effect and photocatalysis [2,12]. While the sheeting effect is based on the removal of contaminants and other desirable species via spreading/flow of water over the surface, photocatalysis induces decomposition and subsequent desorption of the surface-adsorbed species in the presence of sunlight and a suitable catalyst.

During photocatalysis, the underlying mechanism is the generation of an electron–hole pair upon irradiation with a photon having energy equivalent to the semiconductor bandgap energy ( $E_g$ ). When energy greater than the bandgap is provided, these electron–hole pairs diffuse out to the surface and act as electron donors and acceptors. These electrons and holes chemically react with the molecules adsorbed on the surface to create free radicals. Hydroxyl radical is one of the most active initiators of photocatalytic oxidation of organic molecules. These radicals transform organic dirt into water and  $\text{CO}_2$ . Among a wide range of compositions as possible photocatalysts, titanium dioxide or titania ( $\text{TiO}_2$ ) has been found to be the most commonly used semiconductor as hydrophilic self-cleaning coating [3,12]. Several other semiconductor compounds, however, are also emerging as potential candidates for photocatalysts, for example, zinc oxide ( $\text{ZnO}$ ), vanadium oxide ( $\text{VO}_3$ ) [5], sulfides of zinc and cadmium ( $\text{ZnS}$ ,  $\text{CdS}$ ) [13]. Among them,  $\text{ZnO}$  is the most extensively explored material [7,14–20].

$\text{ZnO}$  is a wide bandgap semiconductor with high photocatalytic activity, high thermal and mechanical stability, and non-toxic nature. It may be a suitable or even better alternative to  $\text{TiO}_2$  due to its similar bandgap value and lower cost [21]. Besides photocatalysis [22–24], it is also being utilized in other functional applications including window layer in thin film solar cells [25], UV and gas sensors [26,27], varistors [28], and other piezoelectric devices [29]. In some cases,  $\text{ZnO}$  films have shown superior photocatalytic degradation performance to  $\text{TiO}_2$ . Furthermore, numerous nanoscale morphologies including nanoparticles, thin films, dumbbell-shaped crystals, micro-/nano-rods, nanowires, and nanopetals have been used to assess the photocatalytic properties of  $\text{ZnO}$  [15,16,27–30]. However, a major drawback of using  $\text{ZnO}$  is its susceptibility to deterioration upon exposure to UV irradiation in aqueous solution, a phenomenon usually referred to as photo-corrosion. To decrease this photo-instability and increase the photocatalytic activity,  $\text{ZnO}$  has been doped with different metals, e.g., Ag, Eu, La-Dy co-doping, Mn, Al [15,17,31–33].

Al-doped  $\text{ZnO}$  film with one atomic percent Al was used as a cathode buffer layer in polymer solar cells for enhanced power conversion efficiency [34,35]. Ajala et al. [36] reported superior UV photocatalytic performance of Al-doped  $\text{ZnO}$  film towards decomposition of a model compound due to surface defects and increased hydrophilicity. In another report, a three-layer configuration of sol-gel spin coated  $\text{ZnO}/\text{AZO}/\text{ZnO}$  film demonstrated enhanced photocatalytic degradation of methylene blue dye under visible light irradiation [37]. Addition of two or more metal dopants into  $\text{ZnO}$  has been reported to greatly improve the photocatalytic behavior through a reduction in electron–hole recombination rate. While most reported studies use certain dopants along with aluminum, there are few investigations that employ other metal dopant combinations [38–41].

Compared to sol-gel derived  $\text{ZnO}:\text{Ag}$  and  $\text{ZnO}:\text{Al}$  powders, reports on the photocatalytic degradation of different dyes, such as methylene blue (MB) using metal-doped  $\text{ZnO}$  thin films, are scarce. Although there are several reports on the metal co-doped  $\text{ZnO}$ , we could not find any research that investigated the effect of both Ag and Al as co-dopants in the  $\text{ZnO}$  films for methylene blue and rhodamine B photocatalysis. Earlier, our group performed sol-gel synthesis of  $\text{ZnO}:\text{Al}$  films for use as a transparent conducting oxide in thin solar cells [42]. In this paper, a comparative study of zinc oxide films doped with aluminum ( $\text{ZnO}:\text{Al}$ ) or silver ( $\text{ZnO}:\text{Ag}$ ) with different concentration levels (0.5 to 1.5 weight percent), and co-doped with 0.5 weight percent of each, was performed to investigate their effect on the photocatalytic degradation of methylene blue (MB) in water under UV irradiation. Furthermore, the effect of dopant type and level on the films' hydrophilicity was investigated. Based on the findings, preliminary investigations on the effectiveness of Ag and Al as co-dopants towards photocatalytic degradation behavior of an industrial organic dye, rhodamine blue (RhB), was assessed and discussed.

## 2. Experimental

### 2.1. Materials

In order to prepare sol solutions for thin film deposition, the following chemicals were used: zinc acetate dihydrate (ZAD,  $\text{Zn}(\text{CH}_3\text{COO})_2 \cdot 2\text{H}_2\text{O}$ ), iso-propanol (i-PrOH), ethanol (EtOH), monoethanolamine (MEA,  $\text{HOCH}_2\text{CH}_2$ ), aluminum chloride hexahydrate (ACH,  $\text{AlCl}_3 \cdot 6\text{H}_2\text{O}$ ), and silver nitrate ( $\text{AgNO}_3$ ). For organic solvent photo-degradation, methylene blue hydrate ( $\text{C}_{16}\text{H}_{18}\text{ClN}_3 \cdot x\text{H}_2\text{O}$ ) was used. All the reagents were of analytical grade purity from Sigma-Aldrich (Saint Louis, MO, USA) and were used without any further treatment.

Over soda-lime glass substrates of  $20 \times 20 \text{ mm}^2$  size, thin films of intrinsic and Al- or Ag-doped ZnO were produced. The substrates were cleaned using 2 wt.% chromic acid solution followed by ultrasonic treatment in methanol and finally a thorough rinse in deionized water. Prior to the spin coating, the substrates were dried in a laboratory oven at  $100 \text{ }^\circ\text{C}$  for 15 min.

### 2.2. Precursor Sol Preparation and Film Deposition

The precursor sol was made following the procedure described elsewhere [42]. Briefly, a 0.2 M Zn solution was prepared by dissolving ZAD as Zn precursor salt into i-PrOH followed by drop-by-drop addition of MEA as a stabilizing agent in an  $\text{MEA}:\text{Zn}^{2+}$  molar ratio of 0.75. The resulting solution was magnetically stirred for 1 h at room temperature until a clear homogenous solution was obtained and aged at room temperature for 24 h. For Al doping (ZnO:Al), a separate solution of 0.2 M Al was prepared by dissolving ACH in EtOH and the drop-by-drop addition of MEA as a stabilizing agent in the desirable ZnO:Al molar ratio. The solution mixture was stirred for 1 h at room temperature until a clear homogenous solution was obtained. Both solutions were mixed by adding Al solution into ZnO solution to get Al content in the ZnO films by 0.5, 1.0, and 1.5 weight percent. Similarly, 0.2 M Ag solution was prepared by dissolving  $\text{AgNO}_3$  in EtOH and added to the ZnO solution to produce Ag-doped ZnO (ZnO:Ag) films containing 0.5, 1.0, and 1.5 weight percent Ag. On the molar basis, these compositions correspond to 1.6, 3.2 and 5.1 mol percent for ZnO:Al films and 0.4, 0.8 and 1.3 mol percent for ZnO:Ag thin films. Another sample containing 0.5 weight percent of Ag and Al each and 0.4 and 1.6 mol percent for Ag and Al, respectively, was prepared and explored for photocatalytic degradation of methylene blue (MB) and rhodamine blue.

The films were deposited via static spin coating method. Using a spin coater (Cookson, SCS G3-8 Spincoat, Providence, RI, USA), about  $40 \text{ }\mu\text{L}$  precursor solution was dispensed over the substrate followed by spin coating at 3000 rpm for 15 s and drying in the oven at  $100 \text{ }^\circ\text{C}$ . This process was repeated three times to achieve a reasonable film thickness. The intrinsic and Ag- or Al-doped ZnO films were annealed for 1 h at atmospheric pressure and  $400 \text{ }^\circ\text{C}$  temperature. The sample identification scheme and the functional properties measurement during this work have been listed in Table 1. All the stages of sol preparation, thin films deposition, and annealing are illustrated in Figure 1.

**Table 1.** Sample identification scheme, surface roughness parameters, and other properties of intrinsic and doped ZnO films.

| Sample ID | Description          | $R_a$ (nm) | $R_q$ (nm) | Bandgap $E_g$ (eV) | Contact Angle $\theta$ ( $^\circ$ ) | Rate Constant $k_{app}$ ( $\text{h}^{-1}$ ) |
|-----------|----------------------|------------|------------|--------------------|-------------------------------------|---|
| i-ZnO     | Intrinsic ZnO        | 2.37       | 3.13       | 3.27               | 64.9                                | 1.44  |
| ZnO:Ag0.5 | ZnO with 0.5 wt.% Ag | 2.09       | 2.97       | 3.26               | 34.2                                | 2.32  |
| ZnO:Ag1.0 | ZnO with 1.0 wt.% Ag | 1.56       | 1.85       | 3.24               | 25.1                                | 2.09  |
| ZnO:Ag1.5 | ZnO with 1.5 wt.% Ag | 1.47       | 1.80       | 3.21               | 19.4                                | 1.73  |
| ZnO:Al0.5 | ZnO with 0.5 wt.% Al | 1.05       | 1.34       | 3.32               | 35.7                                | 2.40  |
| ZnO:Al1.0 | ZnO with 1.0 wt.% Al | 0.94       | 1.15       | 3.36               | 28.3                                | 1.89  |
| ZnO:Al1.5 | ZnO with 1.5 wt.% Al | 0.87       | 1.09       | 3.40               | 21.2                                | 1.50  |

$R_a$ : Average surface roughness;  $R_q$ : Root-mean-square roughness.

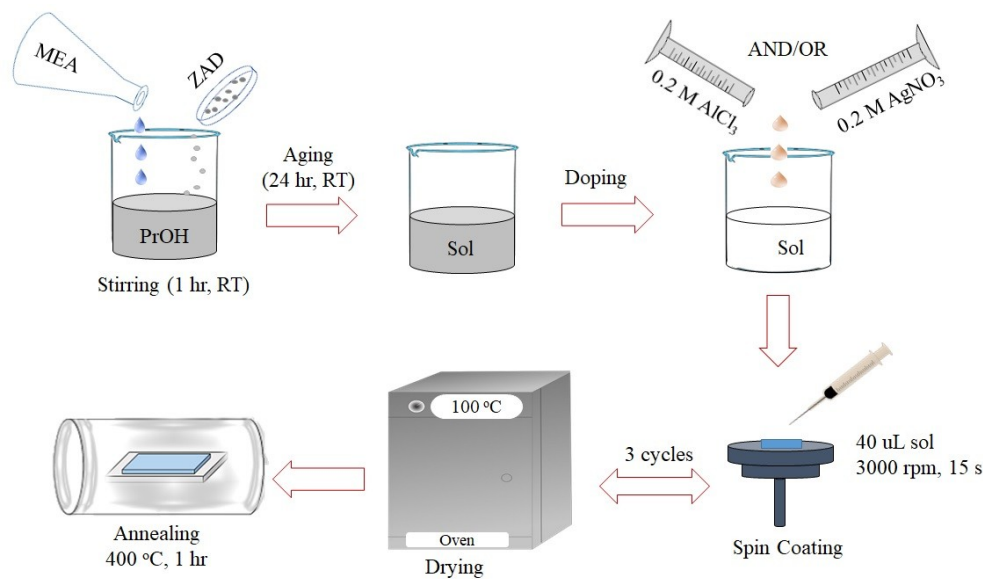


**Figure 1.** Schematic diagram showing different stages of intrinsic and doped ZnO films synthesis.

### 2.3. Photocatalysis of Methylene Blue (MB) and Rhodamine B (RhB)

The MB aqueous solution was prepared using 1 mg MB in 100 mL distilled water. In each beaker, 10 mL of this solution was acquired with the intrinsic or doped ZnO film sample attached to the base. In an enclosed photocatalysis chamber, the measurements were carried out using a UV-C lamp with UV spectrum in the 200–280 nm regime. The extent of MB degradation was determined by taking 4 mL of the solution after 1 h and measuring its absorption at 664 nm ( $\lambda_{\max}$  of MB) for up to 4 h.

For the RhB aqueous solution, 1 mg RhB was added to 100 mL distilled water. The ZnO:(Ag + Al) samples were placed at the base of the beaker containing 10 mL of the RhB solution. The photo-degradation studies were carried out in an enclosed chamber under UV-A light (320–380 nm with peak at 366 nm and a visible light filter). At 1 h intervals, 4 mL of the solution was extracted to determine the extent of RhB degradation through absorption measurements at 553 nm ( $\lambda_{\max}$  for RhB) for up to 10 h.

According to Beer–Lambert law, the concentration of the organic dye or industrial pollutant (MB/RhB) is directly proportional to its absorbance in the solution. The degradation efficiency can be calculated using the equation,

$$\text{Degradation Efficiency} = \frac{C_0 - C}{C_0} \times 100\% = \frac{A_0 - A}{A_0} \times 100\% \quad (1)$$

where  $C_0$ ,  $C$ ,  $A_0$  and  $A$  are the MB concentration and absorbance values initially (at  $t = 0$ ) and after 4 h reaction time, respectively. From the first-order reaction equation, the photocatalysis reaction rate ( $k_{\text{app}}$ ) can be determined, as follows:

$$\ln\left(\frac{C}{C_0}\right) = -kKt = k_{\text{app}}t \quad (2)$$

where  $K$ ,  $k$  and  $t$  are the adsorption constants, the first-order reaction rate constant and irradiation time, respectively. From the best-fit straight line of the semi-logarithmic  $\ln(C/C_0)$  versus  $t$  plot, the value of  $k_{\text{app}}$  as the apparent first-order rate constant may be computed [13].

## 2.4. Characterization and Data Analysis

For topographical examination and surface roughness measurement, the intrinsic (*i*-ZnO) and doped-ZnO films were examined under the atomic force microscope (AFM) (JSPM-5200, JEOL, Tokyo, Japan) through tapping mode operation for the maximum tip-sample interaction. The surface microstructures were viewed under a scanning electron microscope (SEM) (JSM-6490A; JEOL) at 20 kV accelerating voltage and 10 mm working distance. Before SEM studies, a thin conductive layer of gold was applied over the sample surface via sputtering. For crystallographic studies, an X-ray diffractometer (STOE Stadi MP, Darmstadt, Germany) was employed at operating voltage and current of 40 kV and 20 mA, respectively, with a Cu- $k\alpha$  radiation source. The absorbance, transmittance, bandgap energy ( $E_g$ ) as well as refractive index ( $n$ ) values for all the samples were determined using UV-visible spectrophotometer (T60; PG Instruments, Leicestershire, UK). The  $E_g$  values were estimated from  $x$ -intercept of the  $(\alpha h\nu)^2-h\nu$  graph for the samples using the Tauc method. Furthermore, the  $k_{app}$  values for MB degradation by ZnO based samples were computed by considering absorbance values after different reaction times. The wetting characteristics of the different *i*-ZnO, ZnO:Al and ZnO:Ag films was recorded by taking photographs from a camera (Nikon DSLR D5300, Tokyo, Japan) and subsequently estimating the contact angle values using ImageJ software (Version 1.52e) with LBADSA module.

## 3. Results and Discussion

### 3.1. Morphological and Wettability Studies

The high magnification view of the surface microstructure of the *i*:ZnO film after annealing is shown in Figure 2. The microstructure revealed the thin films to be polycrystalline and comprising of fine crystallites with an average size of <50 nm. The film appears smooth and dense throughout. Although isolated surface cracks were seen during the SEM examination, their generation may be attributed to electron beam interaction with the film surface at very high magnification. Although surface cracking in such films may happen due to very low film thickness and rapid solvent removal during spin coating procedure, AFM results (presented in Figure 3) did not indicate their presence in any sample. Furthermore, producing multilayers from multiple spin cast cycles as in this case aptly inhibits the formation of through cracks that would otherwise expose the underlying substrate and adversely affect the film properties.

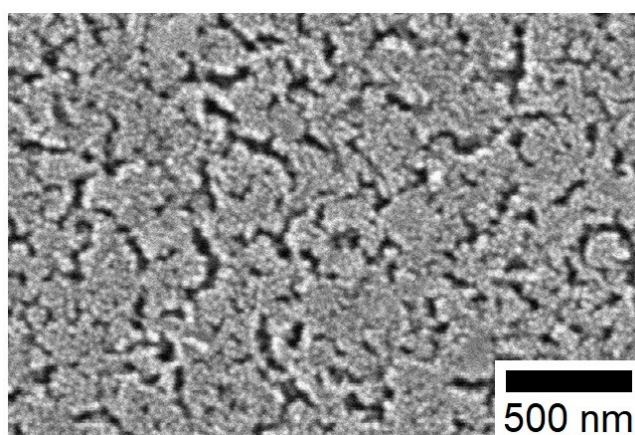
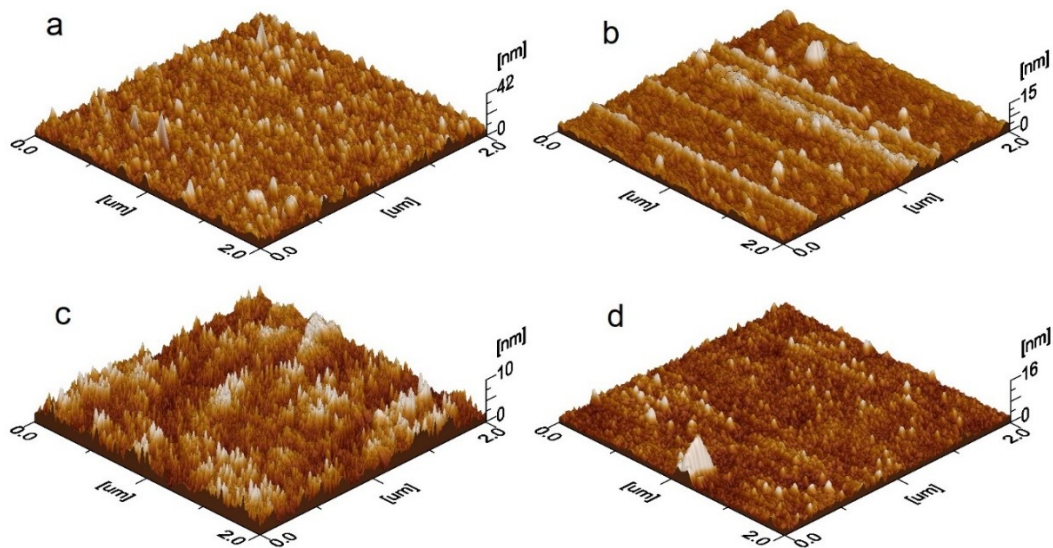


Figure 2. High magnification SEM micrograph of *i*:ZnO thin film.

The effect of Ag- or Au-doping into the ZnO films on the topography was investigated, as presented in Figure 3. While doping with metal ions was found to produce dense, crack-free, smooth films, the grain refinement and the decrease in surface roughness was more pronounced in the case of Al-doping. While an increase in the doping level from 0.5 to 1.5 weight percent did not seem

to strongly influence the grain size, the overall film surface roughness was reduced, particularly in the case of ZnO:Ag films. This may be attributed to a higher density of nucleation centers when spin casting from metal ions containing precursor sols. From X-ray diffraction data, the films were found to exhibit (200) preferred orientation implying c-axis to be parallel to the substrate normal, in agreement with our earlier report [26]. On this length scale, the surface roughness values, listed in Table 1, are of the order of few nanometers, in agreement with other reports [31,32]. The relative difference in atomic radii of the zinc (0.74 Å), silver (1.26 Å) and aluminum (0.535 Å) also introduces lattice distortion in the form of increased dislocation density and lattice strains [33,38].



**Figure 3.** 3D AFM surface topographies of the metal-doped ZnO thin films after annealing: (a) ZnO:Ag0.5; (b) ZnO:Ag1.5; (c) ZnO:Al0.5; and (d) ZnO:Al1.5.

The surface morphology (grain size and roughness) and composition can also be indirectly gauged from surface water contact angle measurements. Depending on the film attributes and illumination conditions, ZnO films may exhibit highly hydrophobic or hydrophilic characteristics [39,40]. The difference in the ionic radii of the Zn and Ag introduces compressive strain in the resulting films, with a reported value of  $0.92 \times 10^{-3}$  for 2 wt.% Ag in ZnO [38]. The water contact angle (CA) values for the intrinsic and silver- or aluminum-doped ZnO films, as determined from sessile water droplets on the film surfaces (Table 1) are graphically represented in Figure 4. While *i*-ZnO film demonstrated somewhat hydrophilic character with a contact angle value of  $64.9^\circ$ , doping with metal ions enhanced the hydrophilicity of the ZnO films to varying extents. The reduction in the CA values may be attributed to an increase in the surface free energy owing to the deteriorated crystallinity in the doped ZnO films. The fact that the extent of CA reduction is greater in the case of ZnO:Al films than those of ZnO:Ag is presumably due to more lattice distortion with maximum reduction by order of three in the case of ZnO:Al-1.5 film.

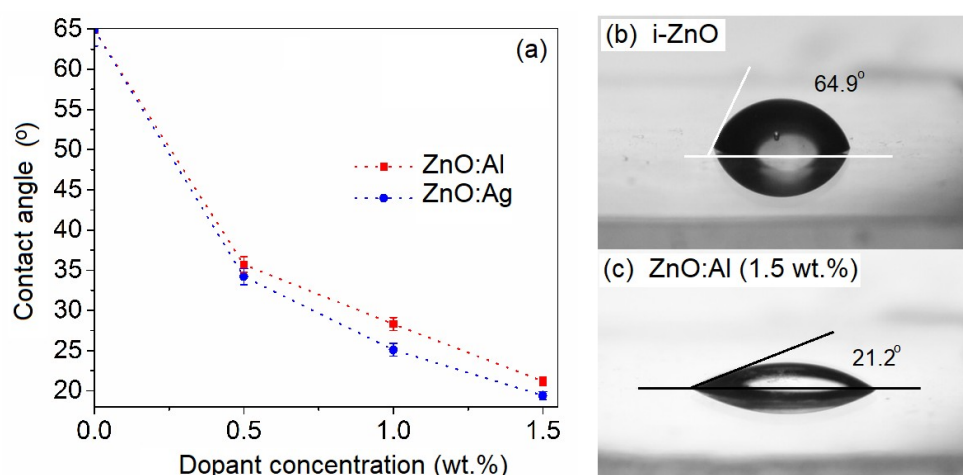


**Figure 4.** (a) Change in contact angle with the increase in the dopant concentration of Al and Ag respectively, (b) shape of water droplets on *i*-ZnO and (c) 1.5 wt.% Al-doped ZnO thin films.

### 3.2. Optical Transmittance and Band Gap Measurements

The optical transmittance spectra of the intrinsic and doped ZnO thin films revealed them to be highly transparent in the visible spectral regime with percent transmittance values of  $\geq 94\%$ , as indicated in Figure 5. In the case of both Ag- and Al-doped ZnO films, an increase in the Ag or Al doping level to 1.5 wt.% resulted in an associated decrease in the percent transmittance from 98% to 94%, presumably due to grain boundary scattering and greater surface defect density. The fundamental absorption edge was found to be positioned at  $\sim 380$  nm, with the sharp drop in absorption near the UV regime owing to the band gap absorption and the electron–hole recombination. Upon increasing the Al concentration, the absorption edge experiences a blue shift, as evident in Figure 5a, which is indicative of greater optical band gap energy, a phenomenon referred to as the Burstein–Moss effect. Briefly, the lower states of the conduction band are filled by excess charge carriers in heavily doped ZnO, causing the Fermi level to move into the conduction band. As the charge carrier concentration increases, the height of the Fermi level in the conduction band increases. According to Pauli Exclusion Principle, a state cannot be occupied by multiple electrons and thus, only electrons which have photon energies greater than the apparent band gap energy can make the transition from the valence band to the conduction band, causing optical band gap widening or the Burstein–Moss shift. On the other hand, a red shift in the absorption edge is noticed upon increasing the Ag concentration in the ZnO films, as evident from Figure 5b. This indicates a decrease in the band gap energy due to the formation of intermediate donor levels below the conduction band with the electrons requiring less energy to move from valence to the conduction band [23]. As demonstrated in Figure 6, the direct band gap energy ( $E_g$ ) values for different ZnO based films were estimated using Tauc method. The values of absorption coefficient ( $\alpha$ ) were calculated from the absorption spectra to obtain  $(\alpha h\nu)^2 - h\nu$  graphs and by extrapolating the linear segment of the curves, the  $E_g$  values were estimated (Table 1). From the values obtained, it was found that the  $E_g$  values for the ZnO:Ag films dropped from 3.272 to 3.208 eV upon increasing the Ag doping level to 1.5 wt.%. Since 2 wt.% corresponds to  $\sim 1.52$  mol% Ag in the ZnO film, the estimated value is very close to the ones reported recently [33]. On the other hand, there was an increase in the  $E_g$  values to 3.397 eV in the case of doping with Al in the ZnO:Al films.

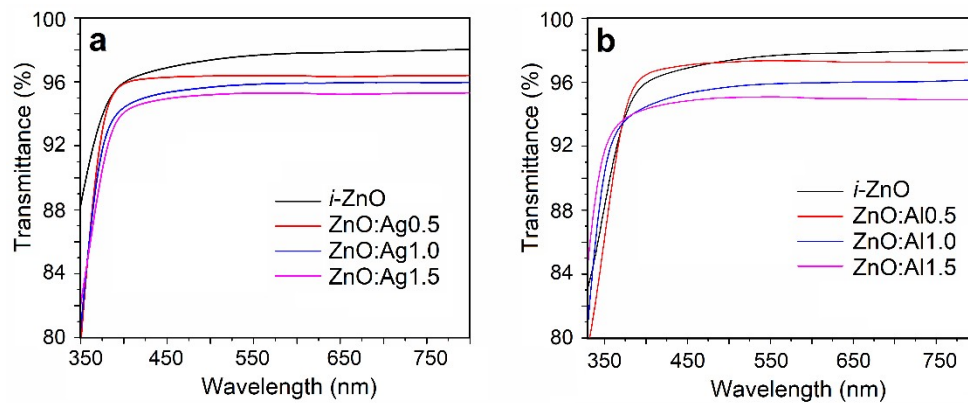


**Figure 5.** Effect of dopant type and concentration on the optical transmission spectra of the ZnO films: (a) Ag-doped ZnO films (ZnO:Ag) and (b) Al-doped ZnO films (ZnO:Al).

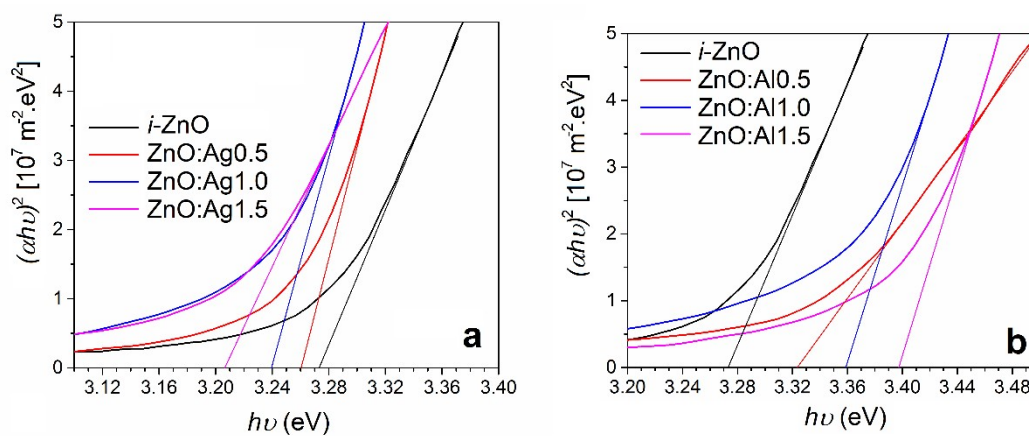


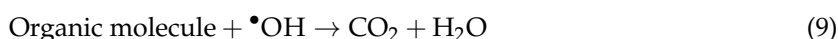
**Figure 6.**  $(\alpha hv)^2$ - $h\nu$  graphs for different ZnO based films to estimate the band gap energy ( $E_g$ ) values: (a) Ag-doped ZnO films and (b) Al-doped ZnO films.

### 3.3. Methylene Blue (MB) Photocatalytic Decomposition

The influence of dopant metal type and concentration on any improvement in the ZnO films photocatalysis behavior was evaluated through degradation of the dye pollutant methylene blue (MB). The process involves irradiation of the ZnO based films with photons having energy equal to or greater than the band gap energy of the films. The electrons jump from the conduction band to the valence band leaving behind a hole. The intensity of the incident photons ( $E = h\nu > E_g$ ) affects the yield of the photogenerated electron and holes. While most of these electrons and holes recombine, a few diffuse to the surface where they either get trapped or react to create radicals. Electrons and holes oxidize or reduce the particles adsorbed on the surface through interfacial charge transfer. Hydroxyl radicals are one of the most active species that oxidize the organic molecules attached to the surface. Oxygen is reduced into superoxide, which leads to the formation of more hydroxyl radicals.

The chemical reactions (3)–(9) represent photon assisted generation of an electron–hole pair and their subsequent roles towards the formation of  $\cdot\text{OH}$ , which subsequently promote decomposition of dye molecules into water and carbon dioxide, as summarized below:





An increase in the number of hydroxyl molecules on the surface of the thin films leads to an increase in the photocatalytic activity. The hydroxyl groups (after irradiation) act as reaction sites, hole traps and the source of hydroxyl radicals.

The results from photocatalysis experiments involving different ZnO thin films are presented in Figure 7. Initially, a pure MB solution was irradiated with UV light without any catalyst to ensure that degradation, if any, was not caused by photocatalysis. The results indicated that MB had decomposed only by 2% in about 4 h, a change too small to be considered significant, caused possibly due to the adsorption of MB on the glass surface. In the case of *i*-ZnO film, the rate of electron–hole pair recombination is high causing the lowest extent of photocatalytic activity. The addition of dopants inhibits the recombination of photogenerated charge carriers by trapping electrons on the surface of the thin films [17]. Using UV-visible spectrophotometer (at 664 nm), the absorbance of the aliquot solution, in liquid cuvette configuration, was monitored after 1 h intervals of UV illumination against deionized water as a reference. According to the Beer–Lambert law, the concentration of MB is directly proportional to the absorbance of MB.

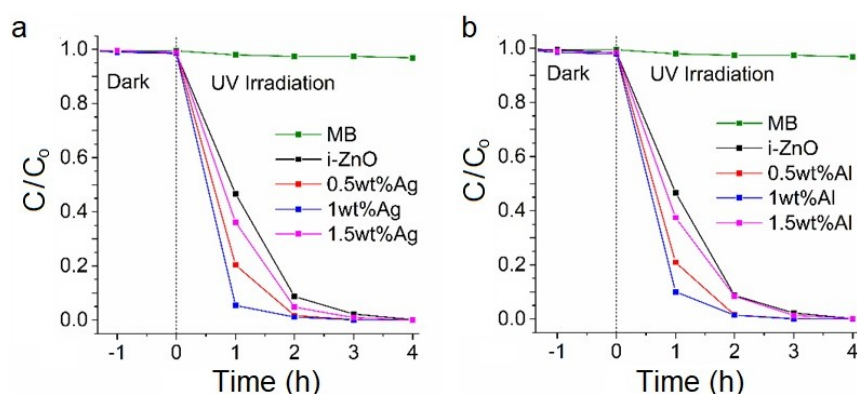


**Figure 7.** Methylene blue concentration after photocatalytic degradation for different times in presence of (a) Ag-doped ZnO films and (b) Al-doped ZnO films.

From Figure 7a, it is evident that after 1 h, while the MB concentration drops to ~47% in the case of *i*-ZnO films, the maximum reduction in C value to  $\leq 5\%$  was obtained for the ZnO:Ag film containing 0.5 wt.% Ag. With longer times, the gap in photocatalytic activities of the different *i*-ZnO and ZnO:Ag films considerably narrowed down. The relatively faster MB degradation rate (Equation (7)) may be attributed to the generation of hydroxyl radicals ( $\cdot\text{OH}$ ) due to the reaction between  $\text{OH}^-$  ions or  $\text{H}_2\text{O}$  molecules and the holes in the valence band (VB) of ZnO (Equations (2) and (3)–(6)). The electron–hole pairs are produced from energy band modulation owing to the difference in work function values for the ZnO (5.2 eV) and Ag (4.26 eV). While degradation efficiency maximizes for 0.5 wt.% doping of Ag in the ZnO, further doping may promote the formation of discrete Ag clusters with a consequent drop in the reaction rate with MB probe dye due to less surface area available for light absorption and reactant adsorption [34,35]. While the ZnO:Al films exhibited similar trend towards photocatalytic degradation of MB (Figure 7b) when compared with the ZnO:Ag films, the MB degradation rate of the latter, however, was greater after 1 h UV illumination, thus indicating the 0.5 wt.% Ag-doped ZnO films to exhibit greater photocatalytic activity.

Comparison of the degradation efficiency values for the intrinsic as well as Ag- or Al-doped films revealed the following trend in photocatalytic activity (from the greatest to the least): 0.5 wt.% (Ag or Al) > 1.0 wt.% (Ag or Al) > 1.5 wt.% (Ag or Al) > *i*-ZnO. Doping ZnO films with Ag was

noticed to be more efficient than Al in terms of enhancement in photodegradation rate of the MB probe dye. Generally, the photodegradation rate of several dyes follows pseudo-first-order kinetics, as proposed by the Langmuir–Hinshelwood model [17,43]. These findings encouraged exploring the effectiveness of both Ag and Al as co-dopants in the ZnO lattice towards photocatalytic degradation of MB. The photocatalytic rate of the ZnO:(0.5Ag + 0.5Al) co-doped ZnO film enhanced to 2.62 h<sup>-1</sup> as compared to both Ag- or Al-doped ZnO samples.

The relative concentration of the MB was plotted against time, on a semi-logarithmic scale, in an attempt to determine the *k*<sub>app</sub> values for different films, as presented in Figure 8. From the graphs, it is evident that all the films followed pseudo-first-order kinetics for MB degradation reaction. From the graphical representation of the data, the values of apparent first-order rate constant for the MB photocatalytic degradation were computed, as listed in Table 1. The *k*<sub>app</sub> values for all the doped ZnO films were found to be greater than that for *i*-ZnO film. The best photocatalytic degradation behavior was demonstrated by ZnO:Ag and ZnO:Al films containing 0.5 weight percent Ag or Al.

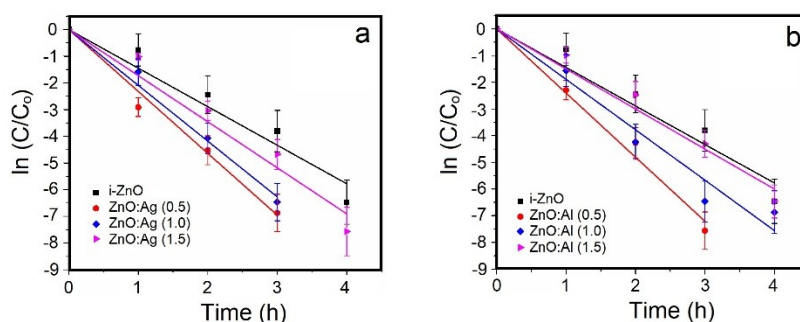
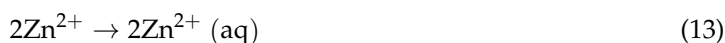
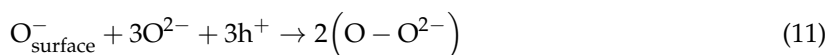


**Figure 8.** Pseudo-first-order plots representing ln(C/C<sub>0</sub>) versus illumination time for calculation of apparent reaction rate constant for MB degradation in the case of: (a) ZnO:Ag films and (b) ZnO:Al films.

### 3.4. Photostability Evaluation of the Doped ZnO Films

The photo-corrosion of ZnO surface occurs mainly because of surface defects. Optimum doping with metal ions may lead to a reduced density of surface defects, which inhibits the photo-corrosion of the thin films. The ZnO film surface deterioration occurs during two slow stages. Initially, a couple of holes are trapped on the film surface, followed by formation of an O<sub>2</sub> molecule and subsequent dissolution as Zn<sup>2+</sup> ions from the surface. The chemical reactions taking place are depicted in Equations (10)–(14) below.



The overall reaction can be represented as:



The extent of photocorrosion in the ZnO-based films was evaluated through their photocatalytic activity over several MB degradation cycles with each cycle lasting for 4 h. For up to five cycles, the degradation efficiency values for the different films were determined after each cycle, as shown in Figure 9. The intrinsic ZnO film performance became quite worse with the maximum drop in the MB photocatalytic degradation efficiency to ~86%. On the other hand, both ZnO:Ag and ZnO:Al

exhibited greater recyclability in terms of less degree of photodegradation for all doping levels with a maximum decrease in efficiency to ~92%. It is interesting to note that except for the second cycle (Figure 9a), ZnO:Ag0.5 and ZnO:Al0.5 samples exhibited superior performance for the first five MB degradation cycles. Even for the other doped films, the decline in activity upon further recycling, as manifested by the decrease in the degradation efficiency, was less drastic than that for intrinsic ZnO. Several factors including the composition change, the active face loss, and the mass loss are considered to be responsible for the reduced recycled activity. In the case of multiple MB photodegradation cycles, selective etching of the ZnO films, in terms of a morphological change from irregular to quasi-rectangular-shaped pores, has been reported and referred to as photocatalytic reaction-induced selective corrosion (PRIS) [44], since it occurs when both UV irradiation and the MB solution are present. Thus, ZnO film loading with Ag or Al has an inhibitory effect, of varying degrees, on Zn<sup>2+</sup> dissolution and selective etching of the active face, with maximum effect induced by an optimal concentration (1 wt.% Ag or Al in this case) and results in high photocatalytic stability. Although it is out of the scope of current work, a detailed microstructural investigation of recycled ZnO-based films may offer a deeper technical insight into the recyclability of such films.

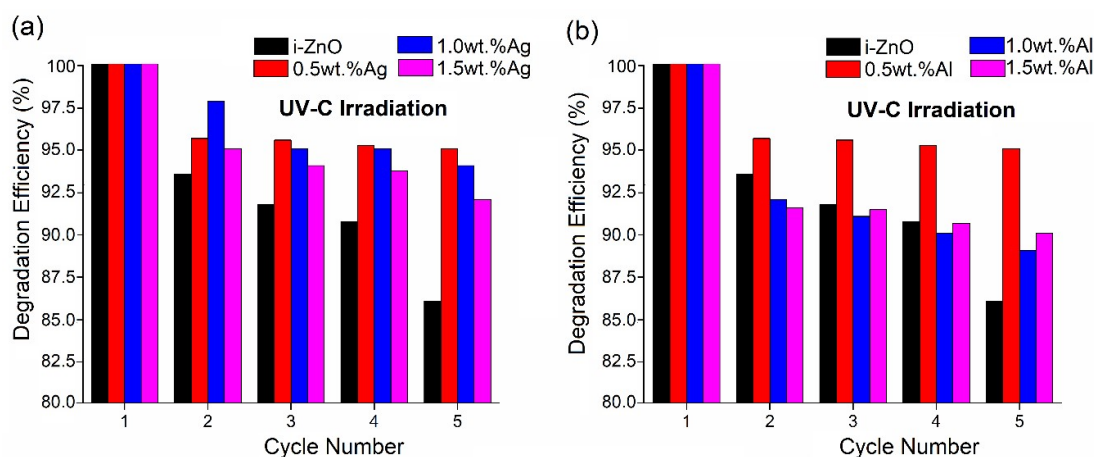


**Figure 9.** Comparison of photostability of *i*-ZnO and doped ZnO films after five runs in MB solution under UV-C irradiation: (a) ZnO:Ag and (b) ZnO:Al.

### 3.5. Photocatalytic Effect of ZnO:(Ag + Al) Film in Rhodamine B Solution

Preliminary investigation into the photocatalytic behavior of Ag and Al co-doped ZnO film was made for the sample containing 0.5 weight percent each for Ag and Al (0.4Ag and 1.4Al mol.%). The co-existence of both Ag and Al into ZnO did not induce any noticeable changes in the film morphology (not shown), presumably due to small amounts of metal dopants. The optical transmittance spectra of the co-doped film (ZnO:0.5Ag + 0.5Al) indicated high percent transmittance of  $\geq 99\%$ , as indicated in Figure S1a. This value is greater than both Ag- and Al-doped ZnO films. The position of the absorption edge was found to be at  $\sim 400$  nm with the sharp drop near the UV regime due to the band gap absorption and the electron–hole recombination. As demonstrated in Figure S1b, the direct band gap energy ( $E_g$ ) value for the co-doped film (ZnO:0.5Ag + 0.5Al), as estimated using Tauc method, was noticed to be  $\sim 3.295$  eV. As compared with the  $E_g$  values for only Ag- or Al-doped ZnO films, the obtained value is higher than that of *i*-ZnO (3.272 eV), but slightly less than that of ZnO:Al0.5 (3.32 eV). In other words, for the same doping level of 0.5 weight percent of Ag and Al, there is an overall blue shift in the absorption edge.

UV illumination of the RhB solution in the presence of this sample indicated an enhancement in the photodegradation rate. The first-order reaction rate constant was determined to be  $0.156 \text{ h}^{-1}$  (compared to  $0.257 \text{ h}^{-1}$  for *i*-ZnO). The relatively low  $k_{app}$  value is considered to be due to the lower energy of the UV lamp. The photocatalytic behavior of the co-doped film against RhB solution,

in terms of concentration change ( $C/C_0$ ) and degradation efficiency (%), is depicted in Figure 10. The film is quite photostable, as evident from Figure 11 since the photodegradation efficiency drops to 92% after five cycles. When compared with other compositions, although the photostability is slightly less than individually doped ZnO films (ZnO:Ag0.5 and ZnO:0.5Al), it is noteworthy that such study was performed in the MB solution for all the other films and under different UV illumination conditions. The results are, nevertheless, very interesting and warrant further experimentation on RhB photodegradation behavior of the co-doped ZnO films.

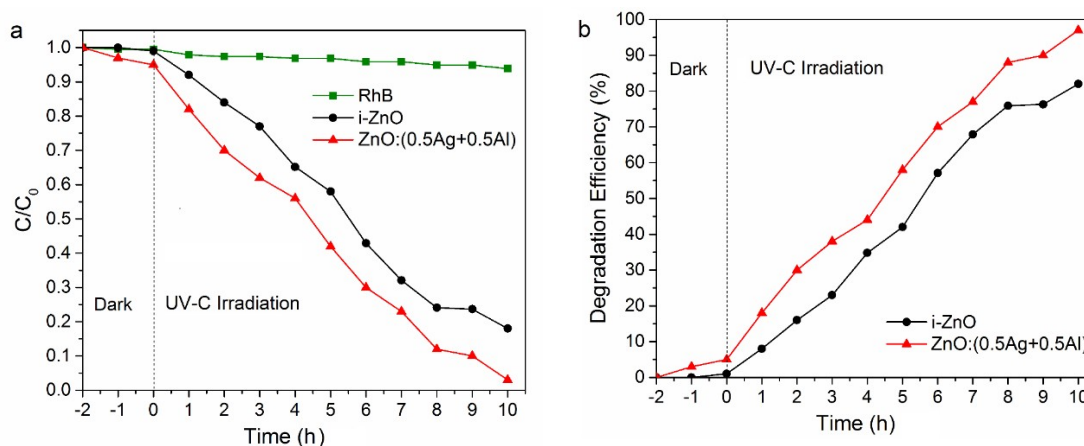


**Figure 10.** Photocatalytic activity of ZnO:Ag + Al film for degradation of rhodamine B under UV-C irradiation: (a) concentration change over time and (b) degradation efficiency.

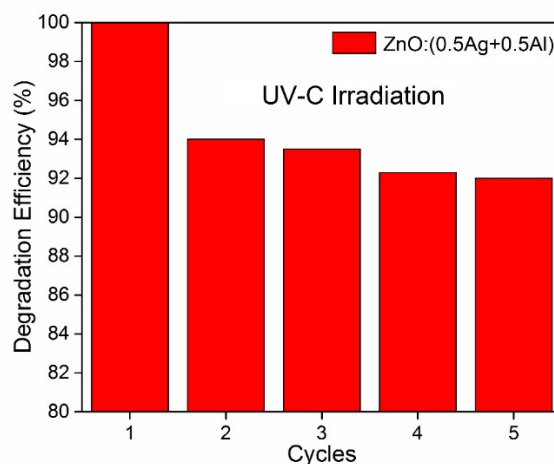


**Figure 11.** ZnO:Ag + Al film stability after several RhB degradation cycles under UV-C irradiation.

#### 4. Conclusions

In this work, highly transparent (>94%) Ag and/or Al-doped ZnO films were produced using sol-gel method and characterized for UV-C photodegradation of methylene blue and rhodamine B. Addition of Ag or Al reduces the solid/liquid interfacial surface energy, thereby causing a drop in the CA value. There is an associated shift in the absorption edge (red for Ag and blue for Al doping) indicating changes in the  $E_g$  values. Such shift and its dependence on film composition may be attributed to the Burstein–Moss effect that introduces the lowest states in the conduction band and their fill-up with electrons due to an increase in the carrier concentration. Ag- or Al-doping enhances the MB degradation efficiency under UV-C irradiation mainly due to an increase in the photogenerated electron–hole pair recombination time and hydroxyl radicals ( $\cdot\text{OH}$ ) generation. The MB degradation followed pseudo-first-order reaction with a maximum value of the apparent reaction rate constant to be  $2.40 \text{ h}^{-1}$  for the ZnO:0.5Al film. The ZnO:(Ag + Al) co-doped film (0.5 wt.% each) offered superior

photocatalytic behavior in both MB and RhB solutions. The photostability and recyclability of the doped ZnO films were superior to those of *i*-ZnO. Dense, nanocrystalline ZnO films doped with small amounts of Ag and/or Al inhibit both Zn<sup>2+</sup> dissolution as well as blocking of the active surface area, thus promoting superior photostability and recyclability.

**Supplementary Materials:** The following are available online at <http://www.mdpi.com/2079-6412/9/3/202/s1>, Figure S1: The optical properties of the co-doped ZnO:Ag + Al film. (a) Transmittance spectrum; and (b) Tauc plot for computation of  $E_g$  value.

**Author Contributions:** Conceptualization, M.A.A. and M.I.; Methodology, A.R., A.A., and H.T.; Validation, I.A. and K.S.; Formal Analysis, H.T., S.J. and M.M.; Investigation, A.R., A.A. and K.S.; Data Curation, I.A. and M.M.; Writing—Original Draft Preparation, A.R., A.A. and H.T.; Writing—Review and Editing, M.A.A. and M.I.; Supervision, S.J. and M.M.; Project Administration, M.A.A., and I.A.; Funding Acquisition, M.I. and S.J.

**Funding:** The authors would like to extend their sincere appreciation to the Deanship of Scientific Research at King Saud University for its funding of this research through the Research Group No. RGP-283. Financial support for this work by the Higher Education Commission of Pakistan through the NRP Grant 6014 is also thankfully acknowledged.

**Acknowledgments:** The authors appreciate the support from the United States Agency for International Development (USAID).

**Conflicts of Interest:** The authors declare no conflict of interest.

## References

- Parkin, I.P.; Palgrave, R.G. Self-cleaning coatings. *J. Mater. Chem.* **2005**, *15*, 1689–1695. [CrossRef]
- Ragesh, P.; Ganesh, V.A.; Nair, S.V.; Nair, A.S. A review on ‘self-cleaning and multifunctional materials’. *J. Mater. Chem. A* **2014**, *2*, 14773–14797. [CrossRef]
- Mellott, N.P.; Durucan, C.; Pantano, C.G.; Guglielmi, M. Commercial and laboratory prepared titanium dioxide thin films for self-cleaning glasses: Photocatalytic performance and chemical durability. *Thin Solid Films* **2006**, *502*, 112–120. [CrossRef]
- Mills, A.; Lepre, A.; Elliott, N.; Bhopal, S.; Parkin, I.P.; O’neill, S.A. Characterisation of the photocatalyst Pilkington Activ™: A reference film photocatalyst? *J. Photochem. Photobiol. A Chem.* **2003**, *160*, 213–224. [CrossRef]
- Liang, Z.; Zhao, L.; Meng, W.; Zhong, C.; Wei, S.; Dong, B.; Xu, Z.; Wan, L.; Wang, S. Tungsten-doped vanadium dioxide thin films as smart windows with self-cleaning and energy-saving functions. *J. Alloy. Compd.* **2017**, *694*, 124–131. [CrossRef]
- Thi, V.H.T.; Lee, B.-K. Development of multifunctional self-cleaning and UV blocking cotton fabric with modification of photoactive ZnO coating via microwave method. *J. Photochem. Photobiol. A Chem.* **2017**, *338*, 13–22. [CrossRef]
- Baudys, M.; Krýsa, J.; Mills, A. Smart inks as photocatalytic activity indicators of self-cleaning paints. *Catal. Today* **2017**, *280*, 8–13. [CrossRef]
- Graziani, L.; Quagliarini, E.; Bondioli, F.; D’Orazio, M. Durability of self-cleaning TiO<sub>2</sub> coatings on fired clay brick façades: Effects of UV exposure and wet & dry cycles. *Build. Environ.* **2014**, *71*, 193–203. [CrossRef]
- Erbil, H.Y.; Demirel, A.L.; Avci, Y.; Mert, O. Transformation of a simple plastic into a superhydrophobic surface. *Science* **2003**, *299*, 1377–1380. [CrossRef]
- Sutha, S.; Suresh, S.; Raj, B.; Ravi, K. Transparent alumina based superhydrophobic self-cleaning coatings for solar cell cover glass applications. *Sol. Energy Mater. Sol. Cells* **2017**, *165*, 128–137. [CrossRef]
- Pathokoti, K.; Manubolu, M.; Hwang, H.-M. Nanotechnology applications for environmental industry. In *Handbook of Nanomaterials for Industrial Applications*; Hussain, C.M., Ed.; Elsevier: Amsterdam, The Netherlands, 2018; pp. 894–907.
- Kalyanasundaram, K. Photochemical applications of solar energy: Photocatalysis and photodecomposition of water. *Photochemistry* **2013**, *41*, 182–265. [CrossRef]
- Soltani, N.; Saion, E.; Hussein, M.Z.; Erfani, M.; Abedini, A.; Bahmanrokh, G.; Navasery, M.; Vaziri, P. Visible light-induced degradation of methylene blue in the presence of photocatalytic ZnS and CdS nanoparticles. *Int. J. Mol. Sci.* **2012**, *13*, 12242–12258. [CrossRef]

14. Intarasuwan, K.; Amornpitoksuk, P.; Suwanboon, S.; Graidist, P. Photocatalytic dye degradation by ZnO nanoparticles prepared from  $X_2C_2O_4$  ( $X = H, Na$  and  $NH_4$ ) and the cytotoxicity of the treated dye solutions. *Sep. Purif. Technol.* **2017**, *177*, 304–312. [[CrossRef](#)]
15. Badawy, M.I.; Mahmoud, F.; Abdel-Khalek, A.A.; Gad-Allah, T.A.; Abdel Samad, A. Solar photocatalytic activity of sol–gel prepared Ag-doped ZnO thin films. *Desalin. Water Treat.* **2014**, *52*, 2601–2608. [[CrossRef](#)]
16. Sun, J.-H.; Dong, S.-Y.; Wang, Y.-K.; Sun, S.-P. Preparation and photocatalytic property of a novel dumbbell-shaped ZnO microcrystal photocatalyst. *J. Hazard. Mater.* **2009**, *172*, 1520–1526. [[CrossRef](#)]
17. Trandafilović, L.; Jovanović, D.; Zhang, X.; Ptasińska, S.; Dramićanin, M. Enhanced photocatalytic degradation of methylene blue and methyl orange by ZnO:Eu nanoparticles. *Appl. Catal. B Environ.* **2017**, *203*, 740–752. [[CrossRef](#)]
18. Xie, W.; Li, Y.; Sun, W.; Huang, J.; Xie, H.; Zhao, X. Surface modification of ZnO with Ag improves its photocatalytic efficiency and photostability. *J. Photochem. Photobiol. A Chem.* **2010**, *216*, 149–155. [[CrossRef](#)]
19. Manzoor, U.; Kim, D.K.; Islam, M.; Bhatti, A.S. Removal of micrometer size morphological defects and enhancement of ultraviolet emission by thermal treatment of Ga-doped ZnO nanostructures. *PLoS ONE* **2014**, *9*, e86418. [[CrossRef](#)]
20. Alam, M.; Islam, M.; Achour, A.; Hayat, A.; Ahsan, B.; Rasheed, H.; Salam, S.; Mujahid, M. Solution processing of cadmium sulfide buffer layer and aluminum-doped zinc oxide window layer for thin films solar cells. *Surf. Rev. Lett.* **2014**, *21*, 1450059. [[CrossRef](#)]
21. Tian, C.; Zhang, Q.; Wu, A.; Jiang, M.; Liang, Z.; Jiang, B.; Fu, H. Cost-effective large-scale synthesis of ZnO photocatalyst with excellent performance for dye photodegradation. *Chem. Commun.* **2012**, *48*, 2858–2860. [[CrossRef](#)]
22. Akram, M.A.; Javed, S.; Islam, M.; Mujahid, M.; Safdar, A. Arrays of czts sensitized ZnO/ZnS and ZnO/ZnSe core/shell nanorods for liquid junction nanowire solar cells. *Sol. Energy Mater. Sol. Cells* **2016**, *146*, 121–128. [[CrossRef](#)]
23. Akram, M.A.; Javed, S.; Xu, J.; Mujahid, M.; Lee, C.-S. Arrays of ZnO/CuIn<sub>x</sub>Ga<sub>1-x</sub>Se<sub>2</sub> nanocables with tunable shell composition for efficient photovoltaics. *J. Appl. Phys.* **2015**, *117*, 205306. [[CrossRef](#)]
24. Shahid, M.; Deen, K.; Ahmad, A.; Akram, M.; Aslam, M.; Akhtar, W. Formation of Al-doped ZnO thin films on glass by sol–gel process and characterization. *Appl. Nanosci.* **2016**, *6*, 235–241. [[CrossRef](#)]
25. Chopra, K.; Paulson, P.; Dutta, V. Thin-film solar cells: An overview. *Prog. Photovolt. Res. Appl.* **2004**, *12*, 69–92. [[CrossRef](#)]
26. Suche, M.; Christoulakis, S.; Moschovis, K.; Katsarakis, N.; Kiriakidis, G. ZnO transparent thin films for gas sensor applications. *Thin Solid Films* **2006**, *515*, 551–554. [[CrossRef](#)]
27. Soci, C.; Zhang, A.; Xiang, B.; Dayeh, S.A.; Aplin, D.; Park, J.; Bao, X.; Lo, Y.-H.; Wang, D. ZnO nanowire UV photodetectors with high internal gain. *Nano Lett.* **2007**, *7*, 1003–1009. [[CrossRef](#)] [[PubMed](#)]
28. Subasri, R.; Asha, M.; Hembram, K.; Rao, G.; Rao, T. Microwave sintering of doped nanocrystalline ZnO and characterization for varistor applications. *Mater. Chem. Phys.* **2009**, *115*, 677–684. [[CrossRef](#)]
29. Özgür, Ü.; Alivov, Y.I.; Liu, C.; Teke, A.; Reshchikov, M.; Doğan, S.; Avrutin, V.; Cho, S.-J.; Morkoç, H. A comprehensive review of ZnO materials and devices. *J. Appl. Phys.* **2005**, *98*, 041301. [[CrossRef](#)]
30. Javed, F.; Javed, S.; Akram, M.A.; Mujahid, M.; Islam, M.; Bhatti, A.S. Surface plasmon mediated optical properties of ZnO/Au/TiO<sub>2</sub> nanoheterostructure rod arrays. *Mater. Sci. Eng. B* **2018**, *231*, 32–39. [[CrossRef](#)]
31. Sakthivel, S.; Neppolian, B.; Shankar, M.; Arabindoo, B.; Palanichamy, M.; Murugesan, V. Solar photocatalytic degradation of azo dye: Comparison of photocatalytic efficiency of ZnO and TiO<sub>2</sub>. *Sol. Energy Mater. Sol. Cells* **2003**, *77*, 65–82. [[CrossRef](#)]
32. Kenanakis, G.; Giannakoudakis, Z.; Vernardou, D.; Savvakis, C.; Katsarakis, N. Photocatalytic degradation of stearic acid by ZnO thin films and nanostructures deposited by different chemical routes. *Catal. Today* **2010**, *151*, 34–38. [[CrossRef](#)]
33. Hsu, J.-C.; Chen, Y.-Y. Comparison of the optical and electrical properties of Al-doped ZnO films using a lorentz model. *Coatings* **2019**, *9*, 4. [[CrossRef](#)]
34. Yu, X.; Zhang, J.; Hu, Z.; Zhao, G.; Zhao, Y. Effective light trapping enhanced near-UV/blue light absorption in inverted polymer solar cells via sol–gel textured Al-doped ZnO buffer layer. *Sol. Energy Mater. Sol. Cells* **2014**, *121*, 28–34. [[CrossRef](#)]

35. Bhattacharya, J.; Peer, A.; Joshi, P.H.; Biswas, R.; Dalal, V.L. Blue photon management by inhouse grown ZnO:Al cathode for enhanced photostability in polymer solar cells. *Sol. Energy Mater. Sol. Cells* **2018**, *179*, 95–101. [[CrossRef](#)]
36. Ajala, F.; Hamrouni, A.; Houas, A.; Lachheb, H.; Megna, B.; Palmisano, L.; Parrino, F. The influence of Al doping on the photocatalytic activity of nanostructured ZnO: The role of adsorbed water. *Appl. Surf. Sci.* **2018**, *445*, 376–382. [[CrossRef](#)]
37. Baradaran, M.; Ghodsi, F.; Bittencourt, C.; Llobet, E. The role of Al concentration on improving the photocatalytic performance of nanostructured ZnO/ZnO:Al/ZnO multilayer thin films. *J. Alloy. Compd.* **2019**, *788*, 289–301. [[CrossRef](#)]
38. Dakhel, A.; Bououdina, M.; Jaafar, A.; Khan, W.; Azam, S.; Minar, J.; Kanoun, M.; Goumri-Said, S. Effect of (Cd, Al) co-doping and hydrogenation on the long-range ferromagnetic ordering of ZnO: Experimental and DFT studies. *J. Alloy. Compd.* **2018**, *753*, 813–820. [[CrossRef](#)]
39. Benzitouni, S.; Zaabat, M.; Aida, M.; Ebothe, J.; Michel, J.; Boudine, B.; Mansouri, L.; Saidani, T. Morphology and photocatalytic activity of porous (In, Mg) co-doped ZnO nanoparticles. *Optik* **2018**, *156*, 949–960. [[CrossRef](#)]
40. Ghomri, R.; Shaikh, M.N.; Ahmed, M.; Song, W.; Cai, W.; Bououdina, M.; Ghers, M. Pure and (Er, Al) co-doped ZnO nanoparticles: Synthesis, characterization, magnetic and photocatalytic properties. *J. Mater. Sci. Mater. Electron.* **2018**, *29*, 10677–10685. [[CrossRef](#)]
41. Thejaswini, T.; Prabhakaran, D.; Maheswari, M.A. Soft synthesis of potassium co-doped Al–ZnO nanocomposites: A comprehensive study on their visible-light driven photocatalytic activity on dye degradation. *J. Mater. Sci.* **2016**, *51*, 8187–8208. [[CrossRef](#)]
42. Salam, S.; Islam, M.; Akram, A. Sol–gel synthesis of intrinsic and aluminum-doped zinc oxide thin films as transparent conducting oxides for thin film solar cells. *Thin Solid Films* **2013**, *529*, 242–247. [[CrossRef](#)]
43. Jongnavakit, P.; Amornpitoksuk, P.; Suwanboon, S.; Ndiege, N. Preparation and photocatalytic activity of Cu-doped ZnO thin films prepared by the sol–gel method. *Appl. Surf. Sci.* **2012**, *258*, 8192–8198. [[CrossRef](#)]
44. Rudd, A.L.; Breslin, C.B. Photo-induced dissolution of zinc in alkaline solutions. *Electrochim. Acta* **2000**, *45*, 1571–1579. [[CrossRef](#)]



© 2019 by the authors. Licensee MDPI, Basel, Switzerland. This article is an open access article distributed under the terms and conditions of the Creative Commons Attribution (CC BY) license (<http://creativecommons.org/licenses/by/4.0/>).